Geoscientific
Model Development
Discussions

Open Access

A flexible three-dimensional stratocumulus, cumulus and cirrus cloud generator (3DCLOUD) based on drastically simplified atmospheric equations and Fourier transform framework

F. Szczap[1], Y. Gour[1], T. Fauchez[2], C. Cornet[2], T. Faure[3], O. Jourdan[1], and P. Dubuisson[2]

[1]Laboratoire de Météorologie Physique, UMR6016, CNRS, Aubière, France
[2]Laboratoire d'Optique Atmosphérique, UMR8518, CNRS, Villeneuve d'Ascq, France
[3]Laboratoire d'Ingénierie pour les Systèmes Complexes, Clermont-Ferrand, France

Correspondence to: F. Szczap (szczap@opgc.univ-bpclermont.fr)

Abstract

The 3DCLOUD algorithm for generating stochastic three-dimensional (3-D) cloud fields is described in this paper. The generated outputs are 3-D optical depth (τ) for stratocumulus and cumulus fields and 3-D ice water content (IWC) for cirrus clouds. This model is designed to generate cloud fields that share some statistical properties observed in real clouds such as the inhomogeneity parameter ρ (standard deviation normalized by the mean of the studied quantity), the Fourier spectral slope β close to $-5/3$ between the smallest scale of the simulation to the outer L_{out} (where the spectrum becomes flat). Firstly, 3DCLOUD assimilates meteorological profiles (humidity, pressure, temperature and wind velocity). The cloud coverage C, defined by the user, can also be assimilated, but only for stratocumulus and cumulus regime. 3DCLOUD solves drastically simplified basic atmospheric equations, in order to simulate 3-D cloud structures of liquid or ice water content. Secondly, Fourier filtering method is used to constrain intensity of ρ, β, L_{out} and mean of τ or IWC of these 3-D cloud structures. 3DCLOUD model was developed to run on a personnel computer under Matlab environment with the Matlab statistics toolbox. It is used to study 3-D interactions between cloudy atmosphere and radiation.

1 Introduction

Clouds have a significant effect on the Earth radiation budget. They reflect the solar radiation and reduce the warming of the Earth (albedo effect). They also create a greenhouse effect by trapping the thermal radiation emitted from the Earth surface, reducing the radiative cooling of the Earth (Collins and Satoh, 2009). Cloud feedback remains however the largest uncertainty in the study of climate sensitivity for almost twenty years (Bony et al., 2006). In almost all climate models, clouds are assumed plane-parallel with homogeneous optical properties (PPH) and radiation codes use one-dimensional (1-D) scheme. Therefore, improving parameterisations of clouds in

large-scale model, especially their interaction with radiation, is a challenge in order to reduce uncertainty in model projections of the future climate (Illingworth and Bony, 2009). Improved global characterization of the three dimensional (3-D) spatial distribution of clouds is thus necessary (Clothiaux et al., 2004).

Moreover, satellite passive and active sensors such as multi-spectral and multi-angular radiometers, LIDAR, RADAR in the A-train mission allow the retrieval of cloud horizontal and vertical optical properties with an adequate spatial and temporal coverage. For practical and computational cost purposes, interpretation of such measurements generally also assumes 1-D radiative algorithm and PPH cloud. This assumption can be far from being realistic and leads to biases on the retrieved properties from passive sensors (Barker and Liu, 1995; Várnai and Marshak, 2002, 2007; Lafont and Guillemet, 2004; Cornet et al., 2005, 2013) and active sensors (Battaglia and Tanelli, 2011). These biases are at least, function of the cloud coverage and of the variability of cloud optical depth or water content. This variability is quantified by an inhomogeneity parameter, often defined as the standard deviation normalized by the mean of the studied quantity (Szczap et al., 2000; Carlin et al., 2002; Oreopoulos and Cahalan, 2005; Sassen et al., 2007; Hill et al., 2012).

Determining the significance of the 3-D inhomogeneity of clouds for climate and remote sensing applications requires to measure and to simulate the full range of actual cloud structure. Set apart the computational time, accurate 3-D cloudy radiative transfer problem is not an issue, per se (Evans and Wiscombe, 2004). Monte Carlo transfer models can indeed accurately and efficiently compute radiative properties for arbitrary cloud fields (Battaglia and Mantovani, 2005; Pincus and Evans, 2009; Mayer, 2009; Cornet et al., 2010; Battaglia and Tanelli, 2011). The difficulty is to generate cloud property fields that are statistically representative of cloud field in nature. Cloud fields generated by dynamic clouds model, like the cloud resolving model (CRM) or the large-eddy simulation model (LES) are very attractive as they contain the state of the art of physical processes (resolution of atmospheric equations, detailed microphysics, radiation,.etc.). Nevertheless, they are very expensive to run in a 3-D domain. Stochastic

◀◀ | ▶▶

◀ | ▶

Back | Close

Full Screen / Esc

Printer-friendly Version

Interactive Discussion

models have the capacity to simulate quickly realistic 2-D and 3-D cloud structures with just a few parameters. Examples of these types of cloud models are: the bounded cascade model (Cahalan et al., 1994; Marshak et al., 1998), the IAAFT algorithm (Venema et al., 2006), the SITCOM model (Di Guiseppe and Thompkins, 2003), the tdMAP model (Benassi et al., 2004), the model developed by Evans and Wiscombe (2004) for low liquid clouds (stratocumulus and cumulus) or by Alexandrov et al. (2010) and the Cloudgen model (Hogan and Kew, 2005) for high ice clouds (cirrus). These stochastic models are based on fractal or Fourier framework. The scale invariant properties observed in real clouds can be controlled. The power spectra of the logarithm of their optical properties (optical depth, liquid water content or liquid water path for low clouds and ice water content for high clouds) typically exhibits a spectral slope of around $-5/3$ (Davis et al., 1994, 1996, 1997, 1999; Cahalan et al., 1994; Benassi et al., 2004; Hogan and Kew, 2005; Hill et al., 2012; Fauchez et al., 2013) from small scale (a few meters) to the "integral scale" or the outer scale (few ten to hundred kilometers), where the spectrum becomes flat (decorrelation occurs). The disadvantage of such model lies in that effects of meteorological processes are poorly considered and dominant scales of organization related to turbulent eddy due, for example, to wind shear, convection, entrainment are not considered.

The aim of the 3DCLOUD algorithm is to reconcile these two approaches. In Sect. 2, we describe the 3DCLOUD generator. In Sect. 3, 3DCLOUD outputs are compared to LES outputs to check the validity of the chosen basic atmospheric equations. In Sect. 4, stratocumulus, cumulus and cirrus examples provided by 3DCLOUD are presented.

2 The 3DCLOUD generator

3DCLOUD generates, in two distinct steps (see Fig. 1), a 3-D optical depth field for stratocumulus and cumulus or a 3-D ice water content field for cirrus clouds. These cloud fields were chosen as most of the papers dealing with scale invariant properties focus on liquid water path and optical depth for stratocumulus and cumulus and

A flexible 3-D stratocumulus, cumulus and cirrus cloud generator

F. Szczap et al.

on ice water content for cirrus. During the first step, meteorological vertical profiles (temperature, pressure, wind, humidity), defined by the user, are assimilated and basic atmospheric equations are resolved. During the second step, cloud scale invariant properties are constrained in a Fourier framework. At the same time, a gamma distribution of local optical depth or IWC is mapped onto the LWC/IWC generated during the first step. This gamma distribution is iteratively computed in such way that the mean optical depth or IWC and the inhomogeneity parameter satisfy the values imposed by the user. Details of these two steps are now presented.

2.1 Step 1: the 3-D LWC/IWC generator

The essential basic quantities to generate cloud fields are the condensed water mixing ratio $q_c = q_l + q_i$ where q_l is the liquid water mixing ratio and q_i is the ice water mixing ratio, the wind velocity vector $\boldsymbol{u}$, air pressure p, temperature T, and vapour water mixing ratio q_v. Mixing ratios are the mass of vapour or condensed water per unit of dry air mass. We describe in this section, the equations used to generate clouds with the associated simplifications used.

2.1.1 The simplification of basic atmospheric equations

The movement of air parcels in the atmosphere is governed by second law of Newton and can be written (Houze, 1993):

$$\frac{\mathrm{d}\boldsymbol{u}}{\mathrm{d}t} = -\frac{1}{\rho}\nabla p - f\boldsymbol{k} \wedge \boldsymbol{u} - g\boldsymbol{k} + \boldsymbol{F} \tag{1}$$

where t is time, ρ the air density, f the Coriolis parameter, g is the acceleration due to gravity and $\boldsymbol{F}$ the acceleration due to other forces (frictional acceleration for example). $\mathrm{d}/\mathrm{d}t = \partial/\partial t + \boldsymbol{u} \cdot \nabla$ is the Lagrangian derivative operator following a parcel of air, $\partial/\partial t$ is the Eulerian derivative operator and ∇ is the three-dimensional gradient operator. $\boldsymbol{u} = u\boldsymbol{i} + v\boldsymbol{j} + w\boldsymbol{k}$ is the wind velocity vector with horizontal components u, v and vertical

A flexible 3-D stratocumulus, cumulus and cirrus cloud generator

F. Szczap et al.

Title Page

Abstract | Introduction

Conclusions | References

Tables | Figures

◄ | ►

◄ | ►

Back | Close

Full Screen / Esc

Printer-friendly Version

Interactive Discussion

component w projected into the Cartesian geometry system, where $\boldsymbol{i}$, $\boldsymbol{j}$ and $\boldsymbol{k}$ are the unit vectors in the x, y and z directions.

When the phase changes are only associated with condensation and evaporation of water, the first law of thermodynamics can be written (Houze, 1993):

$$\frac{\mathrm{d}\theta}{\mathrm{d}t} = -\frac{L}{c_\mathrm{p}\prod}\frac{\mathrm{d}q_\mathrm{v}}{\mathrm{d}t} \tag{2}$$

where $L = 2500\,\mathrm{kJ\,kg^{-1}}$ and $L = 2800\,\mathrm{kJ\,kg^{-1}}$ are the usual latent heat of vaporization of water and ice, respectively. $c_\mathrm{p} = 1.004\,\mathrm{kJ\,kg^{-1}\,K^{-1}}$ is the usual specific heat of dry air at constant pressure, θ is the potential temperature and $\prod = (p/p_0)^\kappa = T/\theta$ is the Exner function where $p_0 = 1000\,\mathrm{hPa}$ and $\kappa = 0.286$.

In addition to the equation of motion and the first law of thermodynamics, parcels of air obey the continuity equation

$$\frac{\mathrm{d}\rho}{\mathrm{d}t} = -\rho\nabla \cdot \boldsymbol{u} \tag{3}$$

and the water continuity equation

$$\frac{\mathrm{d}q_\mathrm{i}}{\mathrm{d}t} = S_i, \qquad i = 1,\ldots,n \tag{4}$$

where S_i are the sum of the sources and sinks for a particular category (among n categories) of water indicated by i (vapor, solid, liquid water category for example).

The horizontal extension of the simulated stratiform cloud fields is around 10 km. We can thus assume a constant horizontal pressure. Moreover, for stratocumulus, cumulus and cirrus clouds fields, the vertical extension of air motions remains confined to a shallow layer, we can apply the Boussinesq approximation, which implies that the atmosphere is an incompressible fluid and the buoyancy forces are function of the virtual potential temperature. At last, we assume an atmosphere characterized by

a high Reynolds number as inviscid fluid and we assume that the Coriolis parameter is negligible. These considerations lead to a dramatically simplification of the dynamic equations. The simplified equations of 3DCLOUD governing the formation of 3-D cloud structures are:

$$\begin{cases} \frac{\mathrm{d}\boldsymbol{u}}{\mathrm{d}t} = g(\frac{\theta_v^*}{\theta_{v0}} - q_c)\boldsymbol{k} \\ \nabla \cdot \boldsymbol{u} = 0 \\ \frac{\mathrm{d}\theta}{\mathrm{d}t} = \frac{L}{c_p \prod} \xi \\ \frac{\mathrm{d}q_v}{\mathrm{d}t} = -\xi \\ \frac{\mathrm{d}q_c}{\mathrm{d}t} = \xi \end{cases} \tag{5}$$

where we denote the reference state by subscript $_0$ and deviation from the reference state by an asterisk, $\theta_v = \theta(1 + 0.61 q_v)$ is the virtual potential temperature. For stratocumulus and cumulus fields ξ is estimated as:

$$\xi = \min(q_{vs} - q_v, q_c)\Delta t \tag{6}$$

where Δt is the simulation time step, the saturation mixing ratio $q_{vs}(T, p)$ is derived from Thetens and Magnus formula and is given by $q_{vs}(T, p) = \frac{0.622 P_{sat}}{(p/100 - 0.378 P_{sat})}$, where for water, $P_{sat} = 6.107 \exp[\frac{4028(T - 273.15)}{234.82(T - 38.33)}]$, and for ice, $P_{sat} = 6.107 \times 10^{[\frac{9.5(T - 273.15)}{265.5 + (T - 273.15)}]}$. Because the saturation mixing ratio q_{vs} is a function of temperature, computation of ξ at each simulation step is based on the work of Asai (1965). For cirrus clouds, condensation, evaporation and ice crystals sedimentation processes are very complex and still not well understood (Karcher and Spichtinger, 2009). In order to take into account supersaturation and sub-saturation regions into cirrus clouds in a very simple way, we used the parameterisation of Starr and Cox (1985) to compute the values of ξ every 2.5 min. Sedimentation processes are taken into account into Eq. (5) by adding ice fall speed

v_{fall} taken from Starr and Cox (1985):

$$v_{fall} = \frac{1.5}{6} \log 10[\max(IWC, 1 \times 10^{-6})] + 1.5 \tag{7}$$

where v_{fall} is in $m\,s^{-1}$ and the ice water content IWC in $g\,m^{-3}$.

2.1.2 Assimilation of meteorological profiles and cloud coverage

In order to control the structure and nature of clouds and especially vertical position and extension, it is necessary to impose a large-scale environment. Practically, forcing terms are added into the 3DCLOUD equations to nudge the solutions towards observations. Our state observations are the initial meteorological profiles (provided by the user for example) and do not change during the simulation. The technique used is based on the initialization integration method (Pielke, 2002). Consequently, 3DCLOUD equations become:

$$\begin{cases} \frac{du}{dt} = G_u(z)\,[u_{ini}(z) - \bar{u}(z)] \\ \frac{dv}{dt} = G_v(z)\,[v_{ini}(z) - \bar{v}(z)] \\ \frac{dw}{dt} = g\left(\frac{\theta_v^*}{\theta_{v0}} - q_c\right) \\ \nabla \cdot \boldsymbol{u} = 0 \\ \frac{d\theta}{dt} = \frac{L}{c_p\Pi}\xi + G_\theta(z)[\theta_{ini}(z) - \theta] \\ \frac{dq_v}{dt} = -\xi + G_{q_v}(z)[q_{v_{ini}}(z) - q_v] \\ \frac{dq_c}{dt} = \xi \end{cases} \tag{8}$$

where for variables X, $\bar{X}(z)$ is the mean of X at height z and quantities $G_X(z)$ are adjusted during the simulation in such a way that X or $\bar{X}(z)$ do not diverge far away from initial conditions $X_{ini}(z)$. In a general way, G is the inverse of timescale but because the contribution of G is artificial, it must not be a dominant term in the governing

Title Page

Abstract | Introduction

Conclusions | References

Tables | Figures

◄ | ►

◄ | ►

Back | Close

Full Screen / Esc

Printer-friendly Version

Interactive Discussion

equations and should be scaled by the slowest physical adjustment processes in the model (Cheng et al., 2001). We first set this timescale to 1 h. Nevertheless, we noticed empirically that 1 h timescale is too large and must be modified as a function of height, especially at height where the vertical gradient of X is large (at the top of a stratocumulus cloud for example). Therefore, we developed a very fast and simple numerical method to adjust the values of $G_X(z)$ during the simulation. At each level, we compute the relative difference $\alpha_X(z) = \frac{X_{\mathrm{ini}}(z) - \overline{X}(z)}{\overline{X}(z)} \cdot 100$. $G_X(z)$ is assumed to be proportional to $\alpha_X(z)$ and is estimated as $G_X(z) = \min[G_{\min} + \frac{G_{\max} - G_{\min}}{\alpha_{X,\max}} \alpha_X(z), G_{\max}]$ where $G_{\min} = \frac{1}{3600}$ s^{-1} and $G_{\max} = \frac{1}{2\Delta t}$. The values of $\alpha_{X,\max}$ were estimated during our numerous numerical experiments. For stratocumulus and cumulus, $\alpha_{X,\max}$ values for horizontal wind, temperature and humidity are 20 %, 2 % and 20 % respectively and for cirrus, $\alpha_{X,\max}$ values are 20 %, 10 % and 10 %, respectively.

The cloud coverage C is defined as the fraction of the number of cloudy pixels to the total number of pixel in the 3DCLOUD field projected onto the 2-D horizontal plan. The value of C is chosen with the assimilation of initial meteorological profiles. At each time step, the initial profile of vapour mixing ratio $q_{v_{\mathrm{ini}}}(z)$ is modified between cloud base and top height if $C \geq 50\%$ or between ground and cloud top height if $C < 50\%$ until C agrees with the desired value within few per cents. The new "initial" profile of vapour mixing ratio $q_{v_{\mathrm{ini}}}^{\mathrm{new}}(z)$ is computed from currently simulated (old) profile of vapour mixing ratio $q_{v_{\mathrm{ini}}}^{\mathrm{old}}(z)$ as $q_{v_{\mathrm{ini}}}^{\mathrm{new}}(z) = q_{v_{\mathrm{ini}}}^{\mathrm{old}}(z) \pm \frac{n_z - n_{\mathrm{base}}}{n_{\mathrm{top}} - n_{\mathrm{base}}} q_{v_{\mathrm{ini}}}^{\mathrm{old}}(z) \times \frac{0.1}{100}$ where z is height, n_z, n_{top} and n_{base} are the index of level in z direction for cloud top height and for cloud base height (or ground), respectively.

This method gives satisfactory results for stratocumulus and cumulus cloud fields (see Sect. 4.1.2) but not for cirrus fields.

Title Page

Abstract | Introduction

Conclusions | References

Tables | Figures

|◀ | ▶|

◀ | ▶

Back | Close

Full Screen / Esc

2.1.3 Implementation of 3DCLOUD algorithm

To implement the previously described equations, space is divided into $(N_x + 2) \times (N_y + 2) \times (N_z + 2)$ cells or voxels where N_x, N_y and N_z are the voxel numbers in each direction. A voxel is characterized by its spatial resolution with $\Delta x = \Delta y \neq \Delta z$. Horizontal extensions are $L_x = L_y$ and can be different of the vertical extension L_z. In order to take account of boundary conditions, one layer of voxel is added around the simulation domain.

We adopted a semi-Lagrangian scheme to solve the equation:

$$\frac{\mathrm{d}X}{\mathrm{d}t} = \frac{\partial X}{\partial t} + \boldsymbol{u} \cdot \nabla X = 0 \tag{9}$$

where X is a scalar advected by the wind velocity $\boldsymbol{u}$. X can be the potential temperature θ, the condensed water q_c or the vapor mixing ratios q_v, and also the three components of wind velocity u, v and w. Two steps are needed in order to compute the value of $X(x, t + \Delta t)$ at a fixed position x and at time $t + \Delta t$. $X(x, t)$ and $\boldsymbol{u}(x, t)$ are known values and Δt is the time step. Firstly, we compute the previous position $p(X, t - \Delta t) = x - \boldsymbol{u}(x, t)\Delta t$ of X at time $t - \Delta t$. Secondly, we compute the value of $X(p, t)$ at the position p and at the time t by an interpolation scheme. This interpolated value $X(p, t)$ is the desired value $X(x, t + \Delta t)$. The major advantage of this approach is that the time step is not restricted by the Courant–Friedrichs–Lewy stability limit but by the less restrictive condition that parcels do not overtake each other during the time step (Riddaway, 2001). Therefore, at each iteration, the maximum value of time step Δt_{max} can be roughly estimated as $\Delta t_{max} = \frac{1}{\max|\frac{\Delta u}{\Delta x}| + \max|\frac{\Delta v}{\Delta y}| + \max|\frac{\Delta w}{\Delta z}|}$. The accuracy of this approach depends on the accuracy of the interpolation scheme. Due to CPU time, we chose a linear interpolation, which unfortunately provides numerical dissipations. However, this drawback is overcome using the Fourier transform performed in the second step of the 3DCLOUD algorithm (see Sect. 2.2.2).

Fourier transform is very easy to implement, we chose thus this method to solve the equation $\nabla \cdot \boldsymbol{u} = 0$. In the Fourier domain, the gradient operator ∇ is equivalent to the

A flexible 3-D stratocumulus, cumulus and cirrus cloud generator

F. Szczap et al.

Full Screen / Esc

Printer-friendly Version

Interactive Discussion

multiplication by ik, where $i \equiv \sqrt{-1}$ and k is the wave number vector. The following equation $ik \cdot \hat{u}(k) = 0$ has thus to be solved, where $\hat{u}$ is the transform of wind velocity u in the Fourier domain. This implies that the Fourier transform of velocity of a divergent free field is always perpendicular to its wave numbers. Therefore, the quantity $1/k^2 (k \cdot \hat{u}(k))k$ is removed from $\hat{u}$. Keeping the real part of inverse transform of $\hat{u}$ provides the new wind velocity u with the desired divergent free property.

Lateral periodic conditions and continuity conditions to bottom and top are applied. For wind velocity, free slip boundary condition is applied at the bottom and top of the domain, which are assumed to be a solid wall (i.e. $w = 0$). But as the Fourier transform (which is needed to solve the equation $\nabla \cdot u = 0$) requires periodic conditions, it provides spurious oscillations during the simulations. In order to limit this effect, extra levels with wind velocity set to zero are added under and above the model domain.

The algorithm of 3DCLOUD in order to simulate 3-D structures of LWC or IWC is, in summary:

1. Definition of initial meteorological profiles u_{ini}, v_{ini}, θ_{ini}, $q_{v_{ini}}$ from idealized cloud conceptual models or from the user. Vertical pressure profile is generally computed from the hydrostatic law but can be provided by the user.

2. Initial perturbations u' are added to wind velocity u. u' is free-divergent and turbulent with a spectral slope of $-5/3$ (see more explanations in Sect. 2.2.2).

3. Assimilation of initial meteorological profiles (optional, see Eq. 8 and Sect. 2.1.2).

4. Constrain of divergent-free velocity u (see Eq. 8).

5. Computation of ice fall speed v_{fall} (only for cirrus cloud, see Eq. 7).

6. Advection of u, v, w, θ, q_v and q_c by wind velocity u (see Eq. 9).

7. Modification of θ, q_v and q_c due to evaporation/condensation processes (see Eq. 6).

A flexible 3-D stratocumulus, cumulus and cirrus cloud generator

F. Szczap et al.

Title Page

Abstract	Introduction
Conclusions	References
Tables	Figures

⏮ ⏭

◄ ►

Back Close

Full Screen / Esc

Printer-friendly Version

Interactive Discussion

8. Modification of the vertical velocity due to buoyancy (see Eq. 8)

9. Modification of $q_{v_{ini}}$ in order to assimilate cloud coverage C (optional, only for stratocumulus and cumulus, see Sect. 2.1.2).

10. Return to Eq. (3) until maximum iteration number is reached.

11. Computation of LWC or IWC, where LWC or IWC = $\rho_{air}q_c$ and ρ_{air} is density of air.

2.2 Step 2: statistical adjustment

We present hereafter the step 2 of 3DCLOUD, the methodology able to adjust, according to user requirements, the mean optical depth $\bar{\tau}$ (or the mean ice water content $\overline{IWC}$) and the inhomogeneity parameter of the optical depth ρ_τ (or the ice water content ρ_{IWC}) from the LWC (or from the IWC) simulated at the step 1. The distribution of τ or IWC is assumed to follow a gamma distribution. Indeed, distribution of τ and IWC could usually be well represented by a lognormal or gamma distribution (Cahalan et al., 1994; Barker et al., 1996; Carlin et al., 2002; Hogan and Illingworth, 2003; Hogan and Kew, 2005). The scale invariant cloud properties are controlled at each level. They are characterised by the spectral exponent β_{1-D} close to $-5/3$ (slope β of the one dimension wave number spectrum in log–log axes of Fourier space) of the local optical depth or the IWC. This spectral slope is computed from the outer scale L_{out} (defined by the user) to the smaller scale (voxel horizontal size).

2.2.1 Control of the mean and of the inhomogeneity parameter

The relation between *local* optical depth $\tau(x,y,z)$, liquid water path LWP and density of water ρ_l in each voxel is given by (Liou, 2002):

$$\tau(x,y,z) = \frac{3}{2\rho_l}\frac{LWP(x,y,z)}{R_{eff}} \text{ with } LWP(x,y,z) = \rho_{air}q_c(x,y,z)\Delta z \qquad (10)$$

where x, y, z are spatial positions inside the simulation domain, LWP(x, y, z) is the *local* liquid water path and Δz is the vertical resolution. *Local* quantity means that the quantity is estimated inside a voxel. The optical depth $\tau(x, y)$ for each pixel is the sum of *local* optical depths along the z axis:

$$\tau(x, y) = \sum_{z=1}^{N_z} (x, y, z). \tag{11}$$

The mean optical depth $\bar{\tau}$ is then defined as:

$$\bar{\tau} = \frac{1}{N_x N_y} \sum_{x=1}^{N_x} \sum_{y=1}^{N_y} \tau(x, y). \tag{12}$$

In the same way, for ice cloud, the mean IWC is obtained with

$$\overline{\text{IWC}} = \frac{1}{N_x N_y N_z^*} \sum_{x=1}^{N_x} \sum_{y=1}^{N_y} \sum_{z=1}^{N_z^*} \text{IWC}(x, y, z) \tag{13}$$

where N_z^* is the number of layer between the cloud top layer and cloud bottom layer.

To describe the amplitude of the optical depth for 1-D and 2-D overcast cloud, Szczap et al. (2000) defined the inhomogeneity parameter of optical depth ρ_τ. For 3-D broken fields, this parameter is defined according to

$$\rho_\tau = \frac{\sigma[\tau^{>0}(x, y)]}{\bar{\tau}^{>0}(x, y)} \tag{14}$$

where $\sigma[\tau^{>0}(x, y)]$ and $\bar{\tau}^{>0}(x, y)$ are the standard deviation and the mean of strictly positive optical depth.

A flexible 3-D stratocumulus, cumulus and cirrus cloud generator

F. Szczap et al.

Title Page

Abstract | Introduction

Conclusions | References

Tables | Figures

|◀ | ▶|

◀ | ▶

Back | Close

Full Screen / Esc

Printer-friendly Version

Interactive Discussion

Due to the flexibility of the mathematical formulation of the gamma distribution and to its ability to mimic the attributes of other positive-value distributions such as lognormal and exponential distribution, we choose to control $\bar{\tau}$ or $\overline{\text{IWC}}$ and ρ_τ or ρ_{IWC} by mapping theoretical gamma-distributed properties onto the simulated properties. This mapping technique is analog to the "amplitude adaptation" technique explained in Venema et al. (2006), where amplitudes are adjusted based on their ranking. The gamma distribution is a two-parameter family of continuous probability distribution. It has a shape parameter a and scale parameter b. The equation defining the probability density as a function of a gamma-distributed random variable Y is:

$$Y = f(\mu; a, b) = \frac{1}{b^a \Gamma(a)} \mu^{a-1} e^{-\mu/b} \tag{15}$$

where $\Gamma(.)$ is the gamma function. We develop a simple iterative algorithm, where values of a and b are adjusted until mean and inhomogeneity parameters reach the required user values within few percent.

2.2.2 Control of invariant scale properties by adjustment of spectral exponent in Fourier space

The spectral slope value $\beta_{\text{1-D}}$ of the horizontally 2-D field is adjusted according to the following methodology. As proposed by Hogan and Kew (2005), we choose to manipulate 2-D plan of Fourier amplitudes of *local* optical depth $\tau_{\text{2-D}}$ (or $\text{IWC}_{\text{2-D}}$) with a 2-D Fourier transform performed at each height of cloudy layer. Suppose a 2-D isotropic field $g(x, y)$ characterized by a Gaussian probability density function (PDF) and a 1-D power spectrum $E_1(k)$ with a spectral slope $\beta_{\text{1-D}}$ at all scales defined as:

$$E_1(k) = \widehat{E_1} k^{-\beta_{\text{1-D}}} \tag{16}$$

where k is the wave number in any direction and $\widehat{E_1}$ is the spectral energy density at $k = 1\,\text{m}^{-1}$. Following Hogan and Kew (2005), for idealized case where $g(x, y)$ is continuous

at small scales and infinite in extend, its 2-D spectral density matrix $E_2(k_x, k_y)$ can be written as

$$E_2(k) = \kappa \widehat{E_1} k^{-\beta_{1\text{-D}}-1} \tag{17}$$

where $k = \sqrt{k_x^2 + k_y^2}$ and κ a constant. In general, a 2-D cloud layer of $\tau_{2\text{-D}}$ (or $IWC_{2\text{-D}}$)

5 is anisotropic and in our case the optical depth (or IWC) is gamma-distributed. Therefore the 1-D power spectrum $E_1(k)$ has seldom the required spectral slope $\beta_{1\text{-D}}$. In this context, a numerical method has to be developed to perform our objectives.

Let set $\widehat{Y_{2\text{-D}}}$ the 2-D Fourier transform of $Y_{2\text{-D}}$, where $Y_{2\text{-D}}$ can be $\tau_{2\text{-D}}$ (or $IWC_{2\text{-D}}$) at a given cloudy layer. This quantity, estimated with the help of a direct 2-D Fast Fourier

10 Transform algorithm can be written as

$$\widehat{Y_{2\text{-D}}}(k) = E_{2\text{-D}}(k) \exp(i\phi_{2\text{-D}}(k)) \tag{18}$$

where $E_{2\text{-D}} = |\widehat{Y_{2\text{-D}}}|$ is the magnitude or spectral energy, $\phi_{2\text{-D}}(k)$ are the phase angles and $k = \sqrt{k_x^2 + k_y^2}$ is the absolute wave number. The cloud field domain is defined to measure L_x and L_y and they have spatial resolutions of Δx and Δy. The resulting

15 wave number for $E_{2\text{-D}}$ ranges from $-K_x$ to $+K_x$ with a resolution of $\Delta k_x = 1/L_x$, where $K_x = 1/2\Delta x$. It is similar for k_y direction.

Our objective is to modify spectral energy $E_{2\text{-D}}(k)$ in such a way that the 1-D spectral slope value $\mu_{1\text{-D}}$ estimated in one dimension from $Y_{2\text{-D}}$ for $k \geq k_{\text{out}}$ ($k_{\text{out}} = 1/L_{\text{out}}$) satisfies the desired value $\beta_{1\text{-D}}$ required by the user. Practically, $\mu_{1\text{-D}}$ is defined as:

20 $$\mu_{1\text{-D}} = (\beta_x + \beta_y)/2 \tag{19}$$

where β_x and β_y are the 1-D spectral slope values of $\widehat{Y_{2\text{-D}}}$ estimated in the x and y directions respectively.

In order to conserve the spatial repartition of $Y_{2\text{-D}}$, we keep $\phi_{2\text{-D}}(k)$ phase angles unchanged for all values of k. We also keep unchanged $E_{2\text{-D}}(k)$ for $k < k_{\text{out}}$. For $k \geq$

k_{out}, two 2-D matrix $E_{2\text{-D}}^{*}(k)$ and $E_{2\text{-D}}^{**}(k)$ can be computed. $E_{2\text{-D}}^{*}(k)$ is based on Eq. (22) and is defined as:

$$E_{2\text{-D}}^{*}(k) = \frac{k^{(-\beta_{1\text{-D}}-1)}}{k_{out}^{(-\beta_{1\text{-D}}-1)}}\overline{E_{2\text{-D}}}(k = k_{out}) \tag{20}$$

whereas $E_{2\text{-D}}^{**}(k)$ is defined as:

$$E_{2\text{-D}}^{**}(k) = \frac{E_{2\text{-D}}(k)}{\overline{E_{2\text{-D}}}(k)}\frac{k^{(-\beta_{1\text{-D}}-1)}}{k_{out}^{(-\beta_{1\text{-D}}-1)}}\overline{E_{2\text{-D}}}(k = k_{out}) \tag{21}$$

where $\overline{X}$ is the mean of variable X. If the degree of anisotropy of $Y_{2\text{-D}}$ is small, such as for stratocumulus and cumulus, we use $E_{2\text{-D}}^{*}(k)$ and if not, such as for cirrus clouds, $E_{2\text{-D}}^{**}(k)$. Nonetheless, the user can also choose one of these methods.

Finally, the new 2-D *local* optical depth (or the 2-D new ice water content $Y_{2\text{-D}}^{new}$) at the given cloudy layer is computed by keeping the real part of the inverse 2-D Fast Fourier Transform of the new quantity:

$$\widehat{Y_{2\text{-D}}^{new}}(k) = E_{2\text{-D}}^{*}(k)\exp(i\phi_{2\text{-D}}(k)) \text{ or } \widehat{Y_{2\text{-D}}^{new}}(k) = E_{2\text{-D}}^{**}(k)\exp(i\phi_{2\text{-D}}(k)) \tag{22}$$

But as a result, the distribution of $Y_{2\text{-D}}^{new}$ is not the same $Y_{2\text{-D}}$ at the given cloudy layer, and the equality between the estimated spectral slope $\mu_{1\text{-D}}$ of $Y_{2\text{-D}}^{new}$ and the required values $\beta_{1\text{-D}}$ is not always guaranteed. Therefore, we have to redo an "amplitude adaptation", as explained in Venema et al. (2006), and to iterate the process explained in this section by changing the value of $\beta_{1\text{-D}}$ in Eqs. (20) or (21), until the estimated value $\mu_{1\text{-D}}$ reaches the required value within few percent.

Title Page

Abstract | Introduction

Conclusions | References

Tables | Figures

◄ | ►

◄ | ►

Back | Close

Full Screen / Esc

Printer-friendly Version

Interactive Discussion

2.2.3 Implementation

We describe here the part of 3DCLOUD algorithm that establishes the cloud field mean optical depth $\bar{\tau}$ ($\overline{\text{IWC}}$), the inhomogeneity parameter ρ_τ (or ρ_{IWC}) and the spectral exponent $\beta_{1\text{-D}}$.

For stratocumulus and cumulus clouds, algorithm is as follows:

1. Transformation of LWC(x,y,z) to $\tau'_{3\text{-D}}(x,y,z)$ with Eq. (10). Effective radius can be set to 10 µm for example.

2. Application of the algorithm explained in Sect. 2.2.2 in order to constrain $\beta_{1\text{-D}}$ of each cloudy layer of $\tau'_{3\text{-D}}(x,y,z)$. We obtain $\tau''_{3\text{-D}}(x,y,z)$.

3. Computation of optical depth $\tau'(x,y)$ from $\tau''_{3\text{-D}}(x,y,z)$ (Eq. 11).

4. Transformation of $\tau'(x,y)$ to $\tau''(x,y)$ with the help of the algorithm explained in Sect. 2.2.1 in order to constrain $\bar{\tau}$ and ρ_τ values.

5. Transformation of $\tau''(x,y)$ to $\tau'''(x,y)$ with the algorithm explained in Sect 2.2.2 in order to control $\beta_{1\text{-D}}$ value.

6. Normalization of $\tau'''(x,y)$ to the required $\bar{\tau}$ value, in order to obtain $\tau_{3\text{-D}}(x,y,z)$.

For cirrus clouds, algorithm is as follows:

1. Transformation of IWC(x,y,z) to IWC$'(x,y,z)$ with the algorithm explained in Sect. 2.2.2 in order to constrain $\overline{\text{IWC}}$ and ρ_{IWC} values.

2. Application of the algorithm explained in Sect. 2.2.2 in order to constrain $\beta_{1\text{-D}}$ of each cloudy layer of IWC$'(x,y,z)$. We obtain IWC$''(x,y,z)$.

3. Transformation of IWC$'''(x,y,z)$ to IWC$_{3\text{-D}}(x,y,z)$ with the algorithm explained in Sect. 2.2.1 in order to constrain $\overline{\text{IWC}}$ and ρ_{IWC} values.

3 Comparison between 3DCLOUD and large-eddy simulation (LES) outputs

The objective of this section is to check that the basic atmospheric equations used in 3DCLOUD (see Sect. 2.1.1) are solved correctly. We compare 3DCLOUD and LES outputs found in the scientific literature for marine stratocumulus, cumulus and cirrus regimes. Note that assimilation techniques of meteorological profiles and of cloud coverage (see Sect. 2.1.2) are not used here.

The test cases come from the output LES numerical files provided by the Global Water and Energy Experiment (GEWEX) Cloud System Studies (GCSS) Working Group 1 (WG1) and Working Group 2 (WG2), easily downloadable from the web. They are often used as benchmark. We choose the DYCOMS2-RF01 case (the first Research Flight of the second Dynamics and Chemistry of Marine Stratocumulus) for the marine stratocumulus regime (Stevens et al., 2005), the BOMEX case (Barbados Oceanographic and Meteorological Experiment) for the shallow cumulus regime (Siebesma et al., 2003), and the ICMCP case (Idealized Cirrus Model Comparison Project) for cirrus regimes (Starr, 2000).

3.1 DYCOMS2-RF01 (GCSS-WG1) case

We remind briefly the conditions of simulations and configurations, explained in detail in Stevens et al. (2005). It was asked to perform a 4 h simulation on a horizontal grid of 96 by 96 points with 35 m spacing between grid nodes. Vertical spacing was required to be 5 m or less. In 3DCLOUD, we set thus $N_x = N_y = 96$ and $N_z = 240$, $L_x = L_y = 3.5$ km and $L_z = 1200$ m, so that $\Delta x = \Delta y \approx 36.5$ m and $\Delta z = 5$ m. Initial profiles of the liquid water potential temperature θ_l and of the total water mixing ratio q_t are $\theta_l = 289.0$ K and $q_t = 9.0$ g kg^{-1} if $z \leq z_i$ and $\theta_l = 297.5 + (z - z_i)^{1/3}$ K and $q_t = 1.5$ g kg^{-1} if $z > z_i$. Other required forcings include geostrophic winds ($U_g = 7$ m s^{-1} and $V_g = -5.5$ m s^{-1}), divergence of the large-scale winds ($D = 3.75 \times 10^{-6}$ s^{-1}), surface sensible heat flux (15 W m^{-2}) and surface latent heat flux (115 W m^{-2}). The momentum surface fluxes

Title Page

Abstract | Introduction

Conclusions | References

Tables | Figures

|◄ | ►|

◄ | ►

Back | Close

Full Screen / Esc

Printer-friendly Version

Interactive Discussion

A flexible 3-D stratocumulus, cumulus and cirrus cloud generator

F. Szczap et al.

where the total momentum is specified by setting $u^* = 0.25\,\mathrm{m\,s^{-1}}$ and the radiation schemes is based on a simple model of the net longwave radiative flux (see Eqs. 3 and 4 in Stevens et al., 2005).

Figure 2 shows the evolution of the mean cloud top height, the mean cloud base height, the cloud coverage and the liquid water path from the master ensemble and for 3DCLOUD during the 4 h simulations. Even though we can notice slight discrepancies between 3DCLOUD and master ensemble results in the first 2 h ("spinup" period), 3DCLOUD results are quite consistent with master ensemble results, especially at the end of the simulation. Nevertheless, 3DCLOUD tends to generate a lower cloud height than the mean results with a higher liquid water path.

Figure 3 shows the mean profiles averaged over the fourth hour of the longwave net flux, the liquid water potential temperature, the total water mixing ratio, the liquid water mixing ratio, the horizontal velocity components, and the air density. Even though the 3DCLOUD longwave net flux is smaller compared to master ensemble, again 3DCLOUD results are quite consistent with others results for all the variables.

3.2 BOMEX (GCSS-WG1) case

For the BOMEX case (Siebesma et al., 2003), it was asked to perform a 6 h simulation on a horizontal grid of 64 by 64 points with 100 m spacing between grid node. Vertical spacing was required to be 40 m. In 3DCLOUD, we set thus $N_x = N_y = 64$ and $N_z = 76$ with $L_x = L_y = 6.4\,\mathrm{km}$ and $L_z = 2980\,\mathrm{m}$, so $\Delta x = \Delta y = 100\,\mathrm{m}$ and $\Delta z \approx 39.2\,\mathrm{m}$. Initial profiles of the liquid water potential temperature θ_l and the total water mixing ratio q_t and the others required forcing including geostrophic winds, divergence due to the subsidence, surface sensible heat flux, surface latent heat flux, momentum surface fluxes, moisture large scale horizontal advection term and longwave radiative cooling (radiative effects due to the presence of clouds are neglected) are presented in Appendix B in Siebesma et al., 2003).

Figure 4 shows the evolution of the cloud coverage and the liquid water path from the master ensemble and for 3DCLOUD during the 6 h simulation. We can notice the small value of the cloud coverage (less than 10 %). 3DCLOUD results are quite consistent with the master ensemble results, even if the simulated 3DCLOUD liquid water path (LWP) may be too low at the end of the simulation.

Figure 5 shows mean profiles averaged over the fifth hours of the cloud coverage, the potential temperature, the water vapour mixing ratio, the liquid water mixing ratio, the horizontal velocity components, and the air density. The 3DCLOUD results are again quite consistent with the master ensemble results. We note however that the 3DCLOUD cloud coverage and liquid water mixing ratio are smaller at any height. We also see small differences (less than $1 \, \mathrm{m \, s^{-1}}$) for the wind velocity for height smaller than 500 m, for the potential temperature (less than 1 K) and for the water vapour mixing ratio (less than $1 \, \mathrm{g \, kg^{-1}}$) for height larger than 1800 m.

3.3 ICMCP (GCSS-WG2) case

For the cirrus case detailed in Starr et al. (2000), the baseline simulations include nighttime "warm" cirrus and "cold" cirrus cases where cloud top initially occurs at $-47\,^{\circ}\mathrm{C}$ and $-66\,^{\circ}\mathrm{C}$, respectively. The cloud is generated in an ice super-saturated layer with a geometric thickness around 1 km (120 % in 0.5 km layer) and with a neutral ice pseudo-adiabatic thermal stratification. Cloud formation is forced via an imposed diabatic cooling over a 4 h time span following by 2 h dissipation stage without cooling. All models simulate radiative transfer, contrary to 3DCLOUD. In 3DCLOUD, we set $N_x = N_y = 60$ and $N_z = 140$ with $L_x = L_y = 6.3$ km and $L_z = 14$ km, so that $\Delta x = \Delta y = 105$ m and $\Delta z \approx 100$ m.

Figure 6 shows the evolution of the ice water path (IWP) from the master ensemble and for 3DCLOUD during the 6 h simulation. In a general way, most of the tested models and 3DCLOUD have similar behaviour: indeed, the IWP increases during the first 4 h simulation (cirrus formation due to imposed cooling) and decreases after (cirrus dissipation due to no imposed cooling). The IWP range of the tested models is

very large (factor of 10), but we can notice that 3DCLOUD behaviour is closer to bulk microphysics models behaviours, especially for "warm cirrus".

For "cold" cirrus, the 3DCLOUD IWP is smaller than most of participating models during all the simulation duration. It is probably because 3DCLOUD do not account for the radiative transfer as opposed to the participating models. Indeed, neglecting cirrus top cooling due to radiative processes restricts the formation of the thin "cold" cirrus. This radiative diabatic effect is probably less important for the "warm" cirrus because the latent heat diabatic effect is larger.

4 Examples of 3DCLOUD possibilities

In this section, we present cloud fields generated by 3DCLOUD with the assimilation of idealized meteorological profiles and fractional cloud coverage defined by the user. We also show the effect of the outer scale L_{out} and the inhomogeneity parameter of optical depth ρ_τ on the generated optical depth field. We also give an example of cirrus clouds with fallstreaks. In order to have a spatial representation of the clouds as seen from above, we choose to show the so-called pseudo-albedo α defined as:

$$\alpha = \frac{(1-g)\tau}{2 + (1-g)\tau} \tag{23}$$

where the asymmetry parameter g is set to 0.86 and τ is the optical depth.

4.1 Stratocumulus and cumulus fields with assimilation of meteorological profiles based on DYCOMS2-RF01 and BOMEX cases

We choose to simulate stratocumulus and cumulus LWC in the context of DYCOMS2-RF01 and BOMEX cases. With this aim, we assimilate temperature and humidity initial profiles for stratocumulus and cumulus given by Stevens et al. (2005) and Siebesma et al. (2003), respectively. However, in order to mimic the sensible and latent heat,

315

Title Page

Abstract | Introduction

Conclusions | References

Tables | Figures

|◀ | ▶|

◀ | ▶

Back | Close

Full Screen / Esc

Printer-friendly Version

Interactive Discussion

these profiles have to be slightly modified. At sea surface ($z = 0$), for stratocumulus (DYCOMS2-RF01 case), the liquid potential temperature and total mixing ratio are set to 290 K and 10 g kg^{-1}, respectively (instead of 289 K and 9 g kg^{-1}, respectively). For cumulus (BOMEX case), the liquid potential temperature is set to 299.7 K instead of 298.7 K. In addition, wind profiles assimilated by 3DCLOUD are those computed by the master ensemble at the end of simulation.

4.1.1 Effects of numerical spatial resolution

The effects of the numerical spatial resolution effects on 3DCLOUD simulations are presented here. Figure 7 shows pseudo-albedo and cross sections of the vertical velocity and cloud water at the end of the simulation for the stratocumulus case based on the DYCOMS2-RF01 experiment. It also shows the mean profiles of potential temperature, liquid water mixing ratio, horizontal velocity components, and vapour water mixing ratio for different numerical spatial resolutions $\Delta x = \Delta y = 200$ m, 100 m, 50 m and 25 m. Horizontal extensions $L_x = L_y$ are set to 10 km and vertical resolution Δz to 24 m for all simulations. Figure 8 is the same as Fig. 7, but for the cumulus case with assimilation of meteorological profiles based on the BOMEX case. The vertical resolution Δz is set to 38.5 m in this last case.

It is obvious that change in the horizontal mesh leads to a more pleasant and detailed flow visualization but there is no significant impact on the mean statistics of the simulated temperature vertical profile, water vapour mixing ration and wind velocity. The water mixing ratio simulated by 3DCLOUD for the DYCOMS2-RF01 case is very close to the mean profile averaged over the fourth hour and provided by master ensemble, even if the vertical resolution used in this section is only $\Delta z = 38.5$ m compared to $\Delta z = 5$ m in Sect. 3.1. For BOMEX case, the water mixing ratio simulated by 3DCLOUD changes as a function of numerical spatial resolution. This behaviour is quite understandable as results drawn on Figs. 7 and 8 are snapshots at the end of the 3DCLOUD simulation and not average results over 1 h as done on Figs. 3 and 5. Moreover, BOMEX

meteorological conditions cause time dependent cumulus fields, contrary to DYCOMS2 meteorological conditions that cause more stationary stratocumulus fields.

Although sensible and latent heat are not prescribed correctly and no radiative transfer scheme is used, 3DCLOUD is able to simulate correctly pertinent cloud statistics, such as temperature, water vapour mixing ratio, wind velocity and in particular cloud water mixing ratio of stratocumulus and cumulus fields, given that the initial meteorological profiles prescribed by the user are representative of the simulated cloud.

4.1.2 Assimilation of the fractional cloud coverage C

Results shown in Fig. 9 are the same results as Fig. 7 with in addition the assimilation of the cloud coverage $C = 99\%$, $C = 80\%$, $C = 50\%$ and $C = 20\%$. Horizontal extensions L_x and L_y are set 10 km and vertical resolution Δz is set to 24 m.

They show that 3DCLOUD is able to assimilate correctly fractional cloud coverage of stratocumulus for very different values of C, even though the extreme example with $C = 20\%$ is a fair weather cumulus field rather than a stratocumulus. For each value of assimilated C, it is interesting to note that cloud base and cloud top heights are still localised around 600 m and 800 m, respectively. Temperature vertical profiles are almost unchanged. The water mixing ratio vertical profiles decrease with the assimilated C value.

4.1.3 Effect of the outer scale L_{out} and inhomogeneity parameter ρ_τ on the optical depth field

We saw that 3DCLOUD can, at the end of the step 1, simulate stratocumulus and cumulus fields with enough coherent statistics profiles. However, optical depth (for stratocumulus and cumulus) or IWC (for cirrus) generated in the step 1 of 3DCLOUD does not show scale invariant properties observed in real cloud and often characterised by the spectral exponent $\beta_{1\text{-D}}$ close to $-5/3$. As described in Sect. 2.2, it is the main task of the step 2 of 3DCLOUD, in addition to the adjustment of the mean and standard

deviation of optical thickness or IWC. We focus on DYCOMS2-RF01 case at the resolution $\Delta x = 50$ m (Fig. 7c). The effective radius R_{eff} is set to 10 µm to compute optical depth from liquid water content. The mean optical depth of this initial field is set to 10 and we change the inhomogeneity parameter ρ_τ and the outer scale L_{out}, respectively, to 0.2 and 1 km for case 1, to 0.7 and 1 km for case 2 and to 0.7 and 10 km for case 3. Figure 10 shows pseudo-albedo, mean power spectra, probability density function of optical depth fields, mean vertical profiles of the horizontally averaged optical depth for the three cases and a volume rendering of optical depth.

First, we notice that the pseudo-albedo of the initial optical depth field (see Fig. 10a) is smoother than the pseudo-albedo of case 1, 2, and 3. Between case 1 and 2, we see clearly an increase of the heterogeneity as case 1 is a quasi-homogenous stratocumulus with a small value of $\rho_\tau = 0.2$ and case 2 is more inhomogeneous with a larger value of $\rho_\tau = 0.7$. Between case 2 and 3, we can see the effect of the outer scale. In accordance with smooth variation, the spectral slope of the initial optical depth is close to -3 for the $[10^{-3} : 10^{-2}]$ m^{-1} wavenumber range (Fig. 10e). Case 1, 2 and 3 present the proper spectral slope value of $-5/3$. For case 1 and 2, this slope is obtained for the $[10^{-3} : 10^{-2}]$ m^{-1} wavenumber range, which is coherent with the imposed value of outer scale $L_{out} = 1$ km. For case 3, $L_{out} = 10$ km, so the spectral slope should be $-5/3$ on the $[10^{-4} : 10^{-2}]$ m^{-1} wavenumber range, however we note that this spectral slope value is achieved only for the $[5 \times 10^{-3} : 10^{-2}]$ m^{-1} wavenumber range. This is due to the fact that we keep unchanged phase angles in the algorithm of 3DCLOUD.

In Fig. 10f, we represent the optical depth distributions. The initial optical depth distribution does not follow common distribution, whereas the distribution of optical depth for case 1 and 2 are log-normal. Indeed, in the 3DCLOUD algorithm, we imposed a gamma distribution on optical depth. For case 2 and 3, optical depth distribution are very close together, even if the outer scale are different. Changing L_{out} value does thus not affect a lot the optical depth distribution shape. In Fig. 10g, we can see that the horizontal mean optical depth profiles are quasi identical for all cases.

These results show undeniably the flexibility of the 3DCLOUD algorithm. Indeed, in step 2, 3DCLOUD is able, by mapping a theoretical gamma-distributed optical depth onto the optical depth field simulated at step1, to adjust, quasi-independently, the optical depth mean value, the inhomogenenity parameter value of optical depth and the spectral slope value of optical depth for $[1/L_{out} : 1/2\Delta x]\,\mathrm{m}^{-1}$ wavenumber range.

4.2 Cirrus fields with assimilation of idealized meteorological profiles

Including some modifications presented in this Sect. 2.1.1, 3DCLOUD is also able to generate cirrus cloud. We briefly present in this section an example of ice water content (IWC) of cirrus with fallstreaks. For cirrus, we chose to generate IWC field instead of optical depth field as for stratocumulus or cumulus.

Figure 11 shows idealized vertical profiles of the potential temperature, the relative humidity, the horizontal velocity components assimilated by 3DCLOUD and the ice water path (IWP) simulated at step 1 by 3DCLOUD. It also shows the IWP simulated by 3DCLOUD during step 2, the initial and corrected mean power spectra, the initial and corrected probability density function and the IWC volume rendering. Horizontal extensions $L_x = L_y$ and vertical extension L_z are set to 10 km and 12.5 km, respectively. Horizontal resolutions $\Delta x = \Delta y$ and vertical Δz are set to 24 m and 83.3 m, respectively. $\overline{\mathrm{IWC}}$ is set to 0.54 mg m^{-3}, the value obtained at the end of step1. The inhomogeneity parameter ρ_{IWC} is set to 1.0 and the outer scale L_{out} is to 1 km.

Initial meteorological profiles assimilated by 3DCLOUD have been constructed in such a way that thin cirrus is generated between 9.5 km and 10.5 km with fallstreaks. Vertical profiles of potential temperature, and especially their vertical gradients under and above the cirrus are based on those proposed by Liu et al. (2003). In order to generate instabilities due to radiative cooling that is not simulated by 3DCLOUD, we imposed a null vertical gradient of the potential temperature near the cirrus top height. We imposed a mean relative humidity with respect to ice (RHI) of 104 % between 9.5 km and 10.5 km. Above cloud, RHI is set to 50 % then 20 % near 12 km, and

under the cirrus, RHI decreases with height to 85 % near 8 km. To generate fallstreaks, we imposed larger wind shear inside the cirrus than under the cirrus.

On Fig. 11, we note that IWP obtained after the step 1 is smoother than IWP after the step 2, and that the initial IWC spectral slope value after step 1 is much smaller (around −5.5) than the corrected IWC spectral slope after the step 2 (around −1.6) in the $[10^{-3} : 2 \times 10^{-2}]\,\text{m}^{-1}$ wavenumber range. For wavenumber smaller than $1/L_{\text{out}} = 10^{-3}\,\text{m}^{-1}$, the power spectra are constant. The corrected IWC probability is exponential-like distribution for step 2. It is due to the larger value of $\rho_{\text{IWC}} = 1.0$ used in this example, compared to $\rho_{\tau} = 0.7$ used for stratocumulus in Sect 4.1.3.

5 Conclusions

3DCLOUD is a flexible three-dimensional cloud generator developed to simulate with a personal computer and under Matlab environment, synthetic but realistic stratocumulus, cumulus and cirrus cloud fields. Simplified dynamic and thermodynamic laws allow the generation of realistic liquid or ice water content from meteorological profiles. Stochastic process with Fourier framework allows us to provide ice water content or optical depth sharing statistical properties with real clouds such as the inhomogeneity parameter (set by the user) and the invariant scale properties characterised by a spectral slope close to −5/3 from the smaller scale (set by spatial resolution of grid computation) to the outer scale (set by the user). In order to simulate cloud structure, 3DCLOUD solves the simplified basic atmospheric equations and assimilates the cloud coverage set by the user (only for stratocumulus and cumulus regime) and meteorological profiles (pressure, humidity, wind velocity) defined by the user.

The 3DCLOUD outputs were compared to the LES outputs for three classical test cases. We chose the case of DYCOMS2-RF01 (the first Research Flight of the second Dynamics and Chemistry of Marine Stratocumulus) for the marine stratocumulus regime (Stevens et al., 2005), the case of BOMEX (Barbados Oceanographic and Meteorological Experiment) for the shallow cumulus regime (Siebesma et al., 2003), and

Full Screen / Esc

Printer-friendly Version

Interactive Discussion

the case of ICMCP (Idealized Cirrus Model Comparison Project) for cirrus regimes (Starr, 2000). For these cases, results show that 3DCLOUD outputs are relatively consistent with LES outputs, and let us confirm that the chosen basic atmospheric equations of 3DCLOUD are solved correctly. We also show that, under the condition that the user provides coherent meteorological profiles for the cloud to be simulated, 3DCLOUD algorithm is able to assimilate them and generate realistic cloud structures.

3DCLOUD is a great tool to understand 3-D interactions between cloudy atmosphere and atmospheric radiation, in order to make progress in the direct radiative problem (GCM context) and in the inverse radiative problem (remote sensing context, development of next generation of atmospheric sensor). For example, 3DCLOUD was used to quantify the impact of stratocumulus heterogeneities on polarized radiation measurements performed by POLDER/PARASOL (Cornet et al., 2013) as well as the influence of cirrus heterogeneities on brightness temperature measured by IIR/CALIPSO (Fauchez et al., 2013).

We still have to develop into 3DCLOUD stochastic process to generate 3-D field of cloud effective radius. In a longer term, investigations will focus on the generation of 3-D mixed phase cloud and eventually on the simulation of 3-D rain rate. Another task will be to provide a FORTRAN code of 3DCLOUD, assumed to be faster than the current Matlab code.

6   Code availability

The source code of the 3DCLOUD algorithm is available online at http://wwwobs. univ-bpclermont.fr/atmos/fr/restricted. Please contact authors for the password.

References

Alexandrov, M. D., Marshak, A., and Ackerman, A. S.: Cellular statistical models of broken cloud fields – Part 1: Theory, J. Atmos. Sci., 67, 2125–2151, doi:10.1175/2010JAS3364.1, 2010.

Asai, T.: A numerical study of the air-mass transformation over the Japan Sea in winter, J. Meteorol. Soc. Jpn., 43, 1–15, 1965.

Barker, H. W. and Liu, D. M.: Inferring optical depth of broken clouds from Landsat data, J. Climate, 8, 2620–2630, 1995.

Barker, H. W., Wiellicki, B. A., and Parker, L.: A parameterization for computing grid-averaged solar fluxes for inhomogeneous marine boundary layer clouds – Part 2: Validation using satellite data, J. Atmos. Sci., 53, 2304–2316, 1996.

Battaglia, A. and Mantovani, S.: Forward Monte Carlo computations of fully polarized microwave radiation in non isotropic media, J. Quant. Spectrosc. Ra., 95, 285–308, 2005.

Battaglia, A. and Tanelli, S.: DOMUS: DOppler MUltiple-Scattering Simulator, IEEE T. Geosci. Remote, 49, 442–450, 2011.

Benassi, A., Szczap, F., Davis, A. B., Masbou, M., Cornet, C., and Bleuyard, P.: Thermal radiative fluxes through inhomogeneous cloud fields: a sensitivity study using a new stochastic cloud generator, Atmos. Res., 72, 291–315, 2004.

Bony, S. R., Colman, R., and Kattsov, V. M.: How well do we understand and evaluate climate change feedback processes?, J. Climate, 19, 3445–3482, 2006.

Cahalan, R. F.: Bounded cascade clouds albedo and effective thickness, Nonlinear Proc. Geophy., 1, 156–167, 1994.

Cahalan, R. F., Ridgway, W., Wiscombe, W. J., Bell, T. L., and Snider, J. B.: The albedo of fractal stratocumulus clouds, J. Atmos. Sci., 51, 2434–2455, 1994.

Title Page

Abstract | Introduction

Conclusions | References

Tables | Figures

◄ | ►

◄ | ►

Back | Close

Full Screen / Esc

Printer-friendly Version

Interactive Discussion

Carlin, B., Fu, Q., Lohmann, U., Mace, G. G., Sassen, K., and Comstock, J. M.: High cloud horizontal inhomogeneity and solar albedo bias, J. Climate, 15, 2321–2339, 2002.

Cheng, W. Y. Y., Wu, T., and Cotton, W. R.: Large-eddy simulations of the 26 November 1991 FIRE II cirrus case, J. Atmos. Sci., 58, 1017–1034, 2001.

Clothiaux, E. E., Barker, H. W., and Korolev, A. V.: Observing clouds and their optical properties, in: 3-D Radiative Transfer in Cloudy Atmospheres, edited by: Marshak, A. and Davis, A. B., Springer, 93–152, 2004.

Collins, W. D. and Satoh, M.: Simulating global clouds, past, present, and future, in: Clouds in the Perturbed Climate System, edited by: Heintzenberg, J. and Charlson, R. J., MIT Press, 469–486, 2009.

Cornet, C.-C., Buriez, J., Riedi, J., Isaka, H., and Guillemet, B.: Case study of inhomogeneous cloud parameter retrieval from MODIS data, Geophys. Res. Lett., 32, L13807, doi:10.1029/2005GL022791, 2005.

Cornet, C., Labonnote, L.-C., and Szczap, F.: Three-dimensional polarized Monte Carlo atmospheric radiative transfer model (3DMCPOL): 3-D effects on polarized visible reflectances of a cirrus cloud, J. Quant. Spectrosc. Ra., 111, 174–186, doi:10.1016/j.jqsrt.2009.06.013, 2010.

Cornet, C., Szczap, F., Labonnote, L.-C., Fauchez, T., Parol, F., Thieuleux, F., Riedi, J., Dubuisson, P., and Ferlay, N.: Evaluation of cloud heterogeneity effects on total and polarized visible radiances as measured by POLDER/PARASOL and consequences for retrieved cloud properties, AIP Conf. Proc., Berlin, 6–10 August 2012, 1531, 99–102, doi:10.1063/1.4804717, 2013.

Davis, A. B., Marshak, A., Cahalan, R. F., and Wiscombe, W. J.: Multifractal characterizations of non-stationarity and intermittency in geophysical fields, observed, retrieved or simulated, J. Geophys. Res., 54, 241–260, 1994.

Davis, A. B., Marshak, A., Wiscombe, W. J., and Cahalan, R. F.: Scale invariance of liquid water distribution in marine stratocumulus – Part 1: Spectral properties and stationarity issues, J. Atmos. Sci., 53, 1538–1558, 1996.

Davis, A. B., Marshak, A., Cahalan, R. F., and Wiscombe, W. J.: The Landsat scale break in Stratocumulus as a three-dimensional radiative transfer effect: implication for cloud remote sensing, J. Atmos. Sci., 54, 241–259, 1997.

Title Page

Abstract | Introduction

Conclusions | References

Tables | Figures

◄ | ►

◄ | ►

Back | Close

Full Screen / Esc

Printer-friendly Version

Interactive Discussion

Davis, A. B., Marshak, A., Gerber, H., and Wiscombe, W. J.: Horizontal structure of marine boundary layer clouds from centimeter to kilometer scales, J. Geophys. Res., 104, 6123–6144, 1999.

Di Giuseppe, F. and Tompkins, A. M.: Effect of spatial organisation on solar radiative transfer in three dimensional idealised stratocumulus cloud fields, J. Atmos. Sci., 60, 1774–1794, 2003.

Evans, K. F. and Wiscombe, W. J.: An algorithm for generating stochastic cloud fields from radar profile statistics, Atmos. Res., 72, 263–289, 2004.

Fauchez, T., Cornet, C., Szczap, F., Dubuisson, P., and Rosambert, T.: Impacts of cirrus clouds heterogeneities on TOA thermal infrared radiation, Atmos. Chem. Phys. Discuss., 13, 27459–27500, doi:10.5194/acpd-13-27459-2013, 2013.

Hill, P. G., Hogan, R. J., Manners, J., and Petch, J. C.: Parametrising the horizontal inhomogeneity of ice water content using CloudSat observations, Q. J. Roy. Meteorol. Soc., 138, 1784–1793, 2012.

Hogan, R. J. and Kew, S. F.: A 3-D stochastic cloud model for investigating the radiative properties of inhomogeneous cirrus clouds, Q. J. Roy. Meteorol. Soc., 131, 2585–2608, 2005.

Houze Jr., R. A.: Cloud Dynamics, Academic Press, San Diego, 1993.

Illingworth, A. and Bony, S. R.: Observational strategies at meso- and large scales to reduce critical uncertainties in future cloud changes, in: Clouds in the Perturbed Climate System, edited by: Heintzenberg, J. and Charlson, R. J., MIT Press, 511–530, 2009.

Kärcher, B. and Spichtinger, P.: Cloud-controling factors of cirrus, in: Clouds in the Perturbed Climate System, edited by: Heintzenberg, J. and Charlson, R. J., MIT Press, 235–268, 2009.

Kobayashi, T.: Effects due to cloud geometry on biases in the albedo derived from radiance measurements, J. Climate, 6, 120–128, 1993.

Lafont, D. and Guillemet, B.: Subpixel fractional cloud cover and inhomogeneity effects on microwave beam-filling error, Atmos. Res., 72, 149–168, doi:10.1016/j.atmosres.2004.03.013, 2004.

Liou, K. N.: An Introduction to Atmospheric Radiation, Academic Press, 2002.

Liu, H.-C., Wang, P. K., and Schlesinger, R. E.: A numerical study of cirrus clouds – Part 2: effects of ambient temperature, stability, radiation, ice microphysics, and microdynamics on cirrus evolution, J. Atmos. Sci., 60, 1097–1119, 2003.

Marshak, A., Davis, A., Wiscombe, W. J., Ridgway, W., and Cahalan, R.: Biases in shortwave column absorption in the presence of fractal clouds, J. Climate, 11, 431–446, 1998.

A flexible 3-D stratocumulus, cumulus and cirrus cloud generator

F. Szczap et al.

Mayer, B.: Radiative transfer in the cloudy atmosphere, European Physical Journal Conferences, 1, 75–99, 2009.

Pincus, R. and Evans, K. F.: Computational cost and accuracy in calculating three-dimensional radiative transfer: results for new implementations of Monte Carlo and SHDOM, J. Atmos. Sci., 66, 3131–3146, 2009.

Pielke, R. A.: Mesoscale Meteorological Modeling, Academic Press, 2002.

Riddaway, R. W.: Numerical methods, available at: www.ecmwf.int/newsevents/training/rcourse_notes/NUMERICAL_METHODS/NUMERICAL_METHODS/Numerical_methods6.html (last access: 10 January 2014), 2001.

Sassen, K., Wang, L., Starr, D. O. C., Comstock, J. M., and Quante, M.: A midlatitude cirrus cloud climatology from the facility for atmospheric remote sensing – Part 5: Cloud structural properties, J. Atmos. Sci., 64, 2483–2501, 2007.

Siebesma, A. P., Bretherton, C. S., Brown, A., Chlond, A., Cuxart, J., Duynkerke, P. G., Jiang, H., Khairoutdinov, M., Lewellen, D., H.-Moeng, C., Sanchez, E., Stevens, B., and Stevens, D. E.: A Large-Eddy Simulation intercomparison study of shallow cumulus convection, J. Atmos. Sci., 60, 1201–1219, 2003.

Starr, D. O. C. and Cox, S. K.: Cirrus clouds – Part 1: A cirrus cloud model, J. Atmos. Sci., 42, 2663–2681, 1985.

Starr, D. O. C., Benedetti, A., Boehm, M., Brown, P. R. A., Gierens, K. M., Girard, E., Giraud, V., Jakob, C., Jensen, E., Khvorostyanov, V. I., Koehler, M., Lare, A., Lin, R.-F., Maruyama, K., Montero, M., Tao, W.-K., Wang, Y., and Wilson, D.: Comparison of cirrus cloud models: a project of the GEWEX Cloud System Study (GCSS) working group on cirrus cloud system, Proceedings of the 13th International Conference on Cloud and Precipitation (ICCP), Reno, NV, USA, 14–18 August, 2000.

Stevens, B., Moeng, H.-C., Ackerman, A. S., Bretherton, C. S., Chlond, A., de Roode, S., Edwards, J., Golaz, J. C., Jiang, H., Khairoutdinov, M., Kirkpatrick, M. P., Lewellen, D. C., Lock, A. L., Müller, F., Stevens, D. E., Whelan, E., and Zhu, P.: Evaluation of large-eddy simulations via observations of nocturnal marine stratocumulus, Mon. Weather Rev., 133, 1443–1462, 2005.

Szczap, F., Isaka, H., Saute, M., Guillemet, B., and Ioltukhovski, A.: Effective radiative properties of bounded cascade nonabsorbing clouds: definition of the equivalent homogeneous cloud approximation, J. Geophys. Res., 105, 20617–20634, doi:10.1029/2000JD900146, 2000.

Title Page

Abstract | Introduction

Conclusions | References

Tables | Figures

◄ | ►

◄ | ►

Back | Close

Full Screen / Esc

Printer-friendly Version

Interactive Discussion

Szczap, F., Cornet, C., Alqassem, A., Gour, Y., Labonnote, C.-L., and Jourdan, O.: A 3-D polarized Monte Carlo LIDAR system simulator for studying effects of cirrus inhomogeneities on CALIOP/CALIPSO measurements, AIP Conf. Proc., Berlin, 6–10 August 2012, 1531, 139–142, doi:10.1063/1.4804727, 2013.

Várnai, T. and Marshak, A.: Observations of three-dimensional radiative effects that influence MODIS cloud optical thickness retrievals, J. Atmos. Sci., 59, 1607–1618, 2002.

Várnai, T. and Marshak, A.: View angle dependence of cloud optical thickness retrieved by MODIS, J. Geophys. Res., 112, D06203, doi:10.1029/2005JD006912, 2007.

Venema, V., Meyer, S., García, S. G., Kniffka, A., Simmer, C., Crewell, S., Löhnert, U., Trautmann, T., and Macke, A.: Surrogate cloud fields generated with the iterative amplitude adapted fourier transform algorithm, Tellus A, 58, 104–120, 2006.

Yang, H., Dobbie, S., Mace, G. G., Ross, A., and Quante, M.: GEWEX Cloud System Study (GCSS) cirrus cloud working group: development of an observation-based case study for model evaluation, Geosci. Model Dev., 5, 829–843, doi:10.5194/gmd-5-829-2012, 2012.

Title Page

Abstract | Introduction

Conclusions | References

Tables | Figures

|◄ | ►|

◄ | ►

Back | Close

Full Screen / Esc

Printer-friendly Version

Interactive Discussion
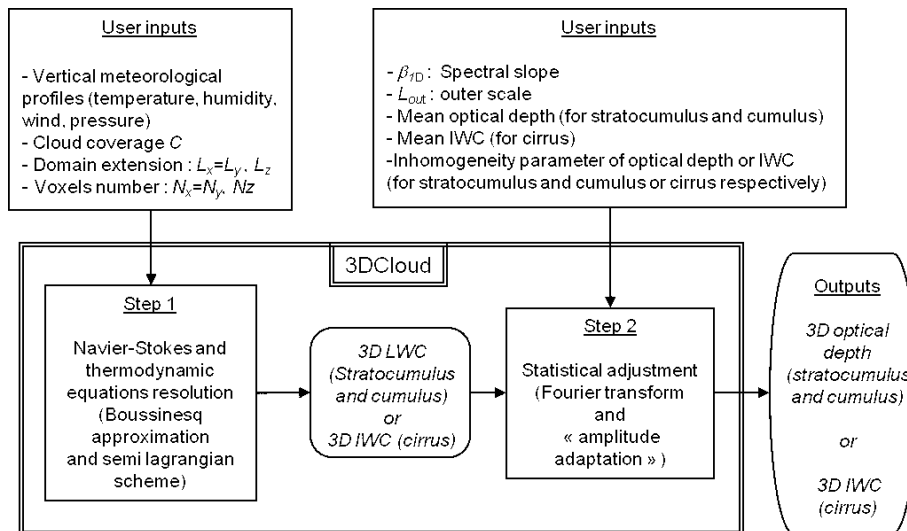
Fig. 1. General flow chart of the stratocumulus, cumulus and cirrus generator 3DCLOUD. Note that 3DCLOUD algorithm is decomposed into two distinct steps.
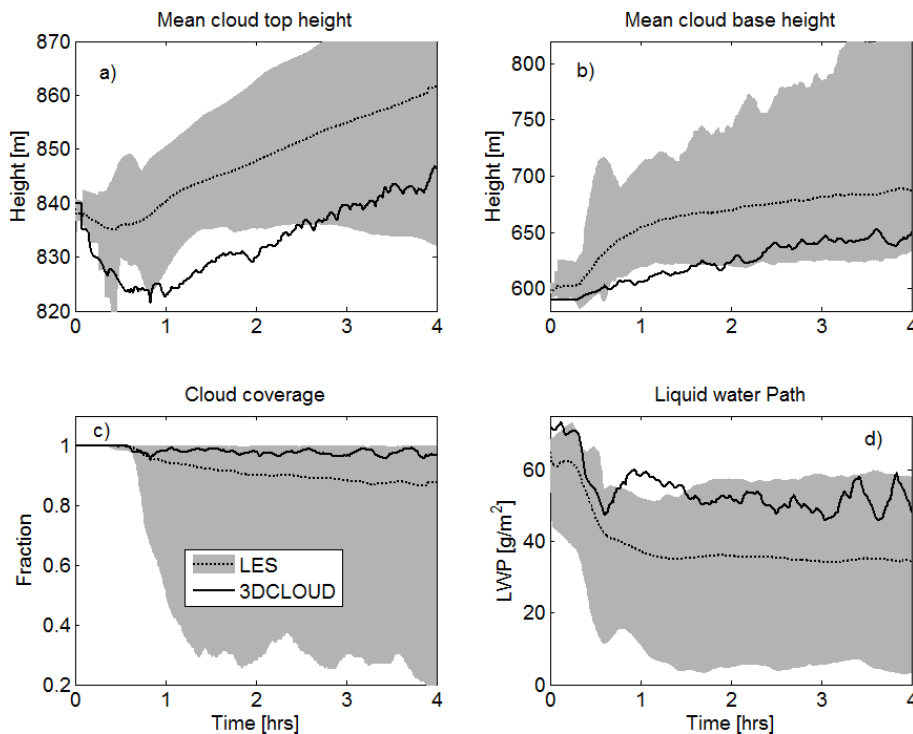
Fig. 2. Time series of **(a)** the mean cloud top height, **(b)** the mean cloud base height, **(c)** the cloud coverage, and **(d)** the liquid water path. The solid lines indicate 3DCLOUD results. The dotted lines indicate a mean over all LES results. The light shading around this mean delimits the maximum and minimum values within the master ensemble at any given time.
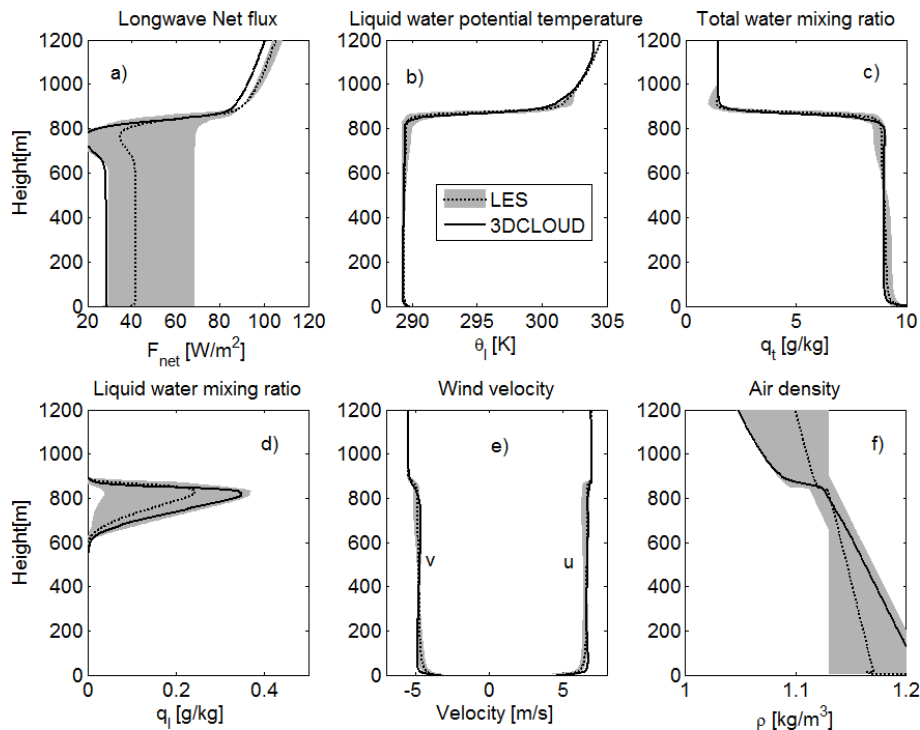
Fig. 3. Mean profiles averaged over the fourth hour of **(a)** the longwave net flux, **(b)** the liquid water potential temperature, **(c)** the total water mixing ratio, **(d)** the liquid water mixing ratio, **(e)** the horizontal velocity components, and **(f)** the air density. The solid lines indicate 3DCLOUD results. The dotted lines indicate a mean over all LES results. The light shading around this mean delimits by the maximum and minimum values within the master ensemble at any given height.
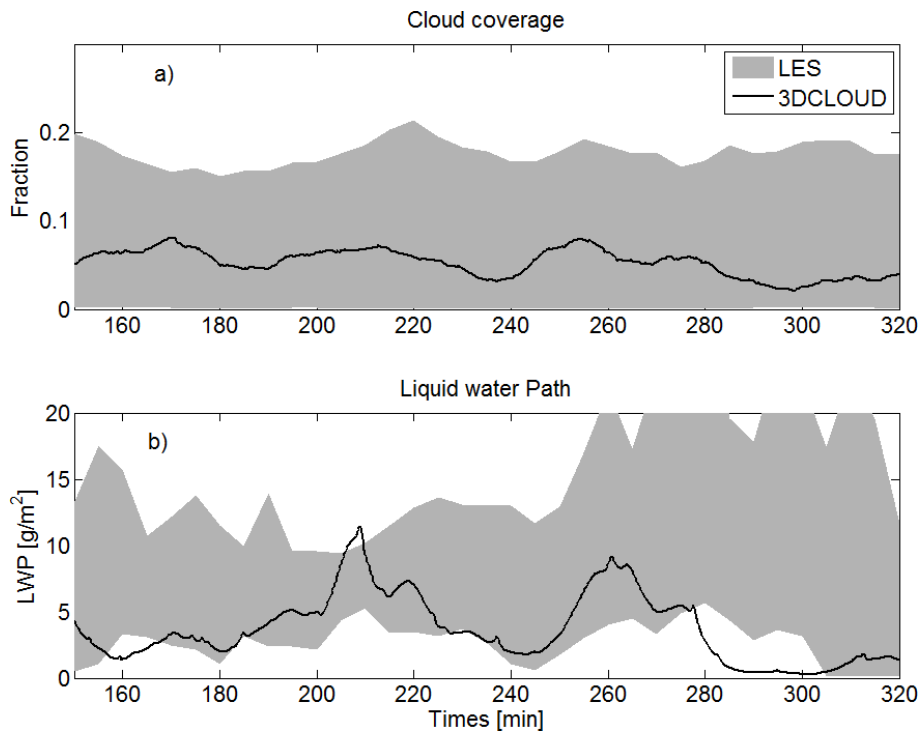
Fig. 4. Time series of **(a)** the cloud coverage and **(b)** the liquid water path. The solid lines indicate 3DCLOUD results. The light shading delimits the maximum and minimum values within the master ensemble at any given time.
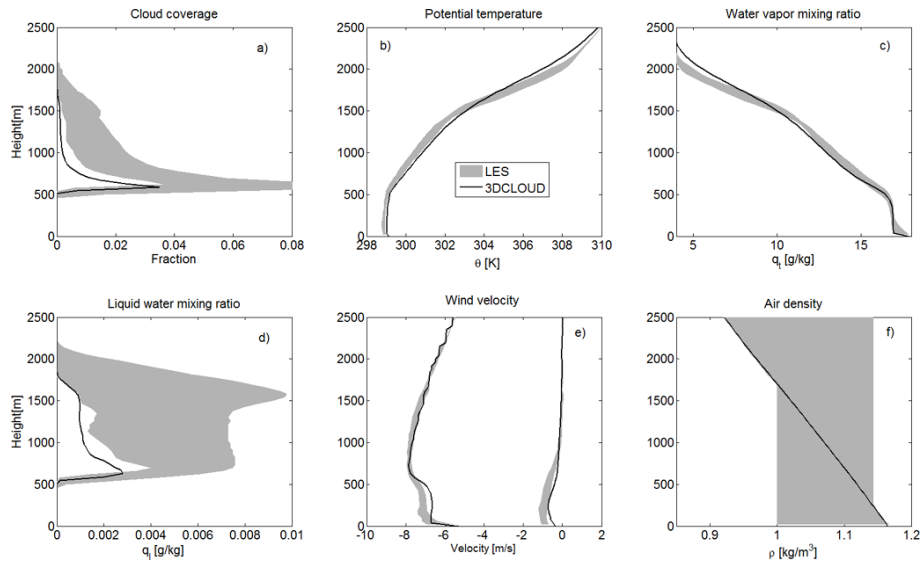
Fig. 5. Mean profiles averaged over the fifth hour of **(a)** cloud coverage, **(b)** the potential temperature, **(c)** the water vapour mixing ratio, **(d)** the liquid water mixing ratio, **(e)** the horizontal velocity components, and **(f)** the air density. The solid lines indicate 3DCLOUD results. The light shading delimits the maximum and minimum values within the master ensemble at any given height.
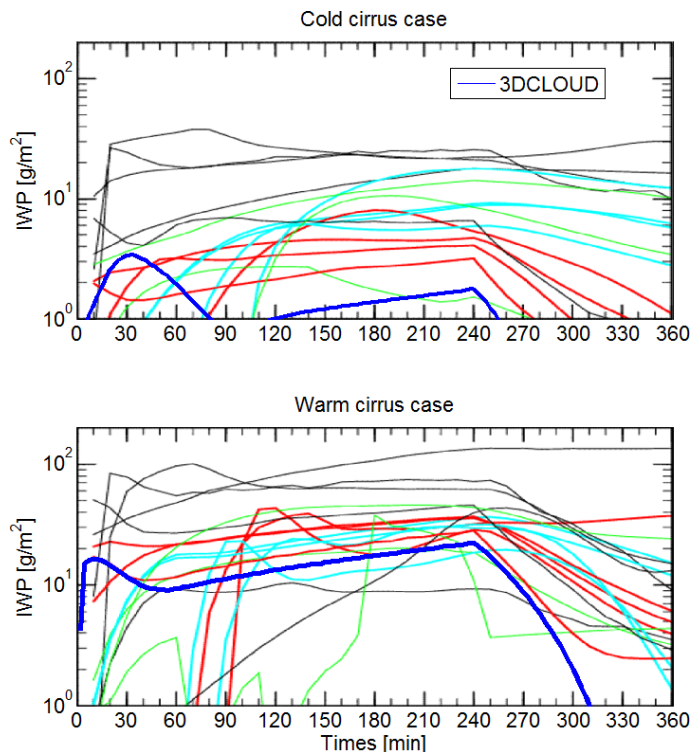
Fig. 6. Time series of vertically-integrated ice water path (IWP) from different cirrus models, which participated to the Idealized Cirrus Model Comparison Project and from the 3DCLOUD model (thick blue lines). The upper panel is for the cold cirrus case and the bottom one is for the warm cirrus case. Cyan represents models with bin microphysics, red models with bulk microphysics, green single column models, and thin black lines models with heritage in the study of deep convection or boundary layer clouds. This figure is made from the one taken from Starr et al. (2000) and Yang et al. (2012).

Title Page

Abstract   Introduction

Conclusions   References

Tables   Figures

|◄   ►|

◄   ►

Back   Close

Full Screen / Esc

Printer-friendly Version

Interactive Discussion
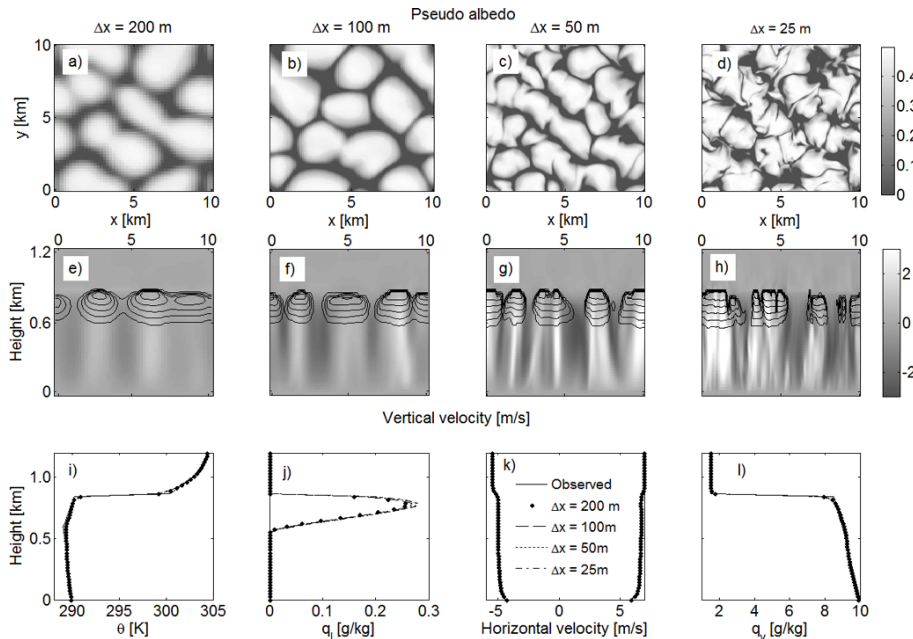
Fig. 7. (a), **(b)**, **(c)** and **(d)** pseudo albedo and **(e)**, **(f)**, **(g)**, and **(h)** cross sections of the vertical velocity (shaded) and the cloud water (contoured), at the end of simulation, for the stratocumulus simulated by 3DCLOUD with assimilation of meteorological profiles based on DYCOMS2-RF01 case. Different numerical spatial resolutions are presented with $\Delta x = \Delta y$: **(a)** and **(e)** $\Delta x = 200$ m, **(b)** and **(f)** $\Delta x = 100$ m, **(c)** and **(g)** $\Delta x = 50$ m and **(d)** and **(h)** $\Delta x = 25$ m. **(i)**, **(j)**, **(k)** and **(l)** mean profiles of the potential temperature, the liquid water mixing ratio, the horizontal velocity components, and the vapour water mixing ratio. The solid lines indicate meteorological profiles based on DYCOMS2-RF01 case and assimilated by 3DCLOUD. Points, dotted lines, dashed lines and dash-dot lines indicate 3DCLOUD results at the end of simulation for that different numerical spatial resolution $\Delta x = 200$ m, $\Delta x = 100$ m, $\Delta x = 50$ m and $\Delta x = 25$ m, respectively.
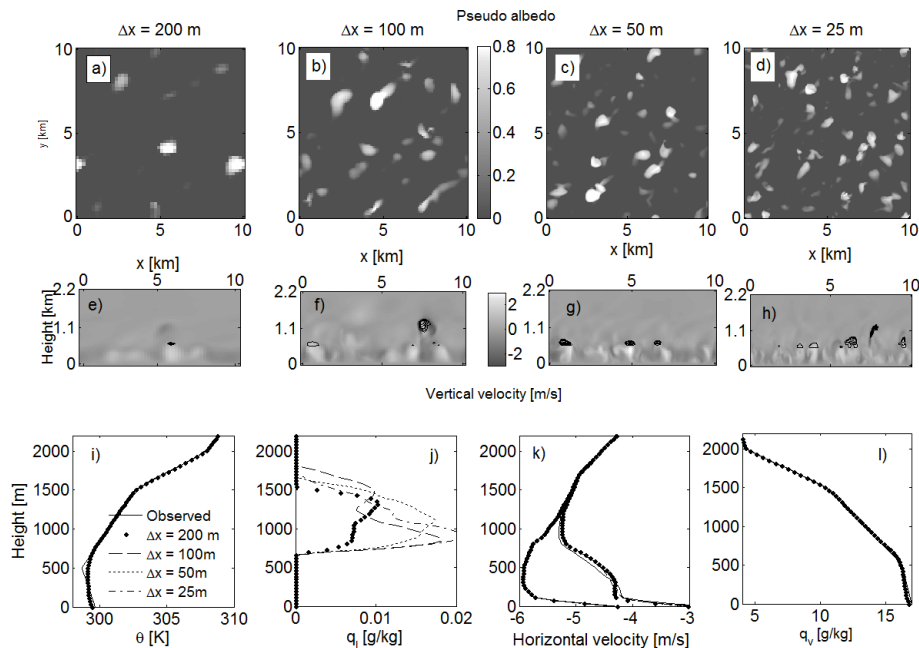
Fig. 8. Same as Fig. 7, for cumulus cloud simulated by 3DCLOUD with assimilation of meteorological profiles based on the BOMEX case.
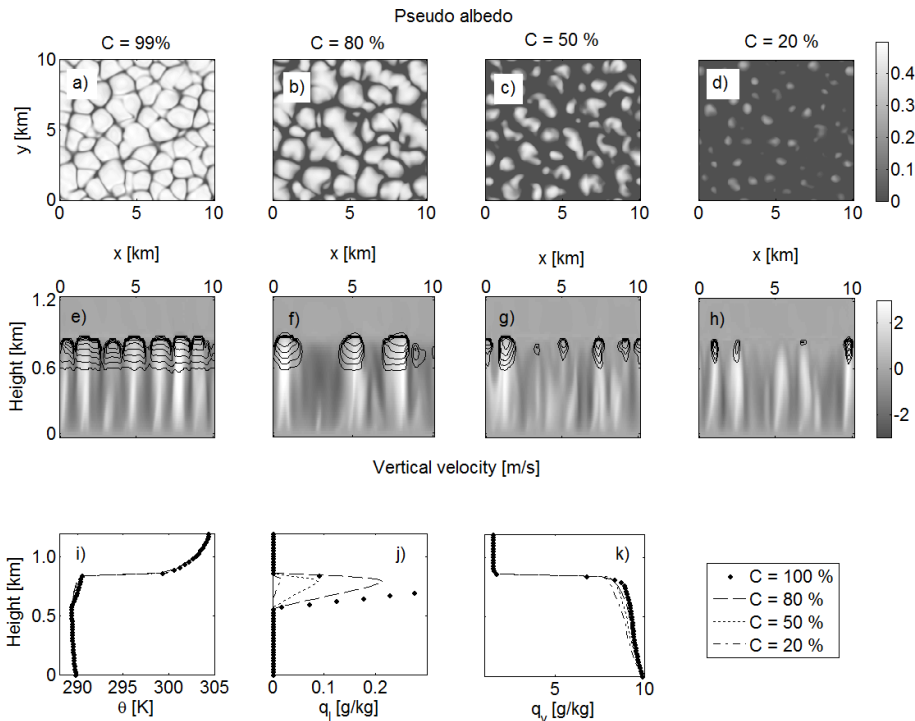
Fig. 9. Same as Fig. 7c ($\Delta x = 50$ m), for different assimilated values of the cloud coverage: **(a)** and **(e)** $C = 99$%, **(b)** and **(f)** $C = 80$%, **(c)** and **(g)** $C = 50$% and **(d)** and **(h)** $C = 20$%.
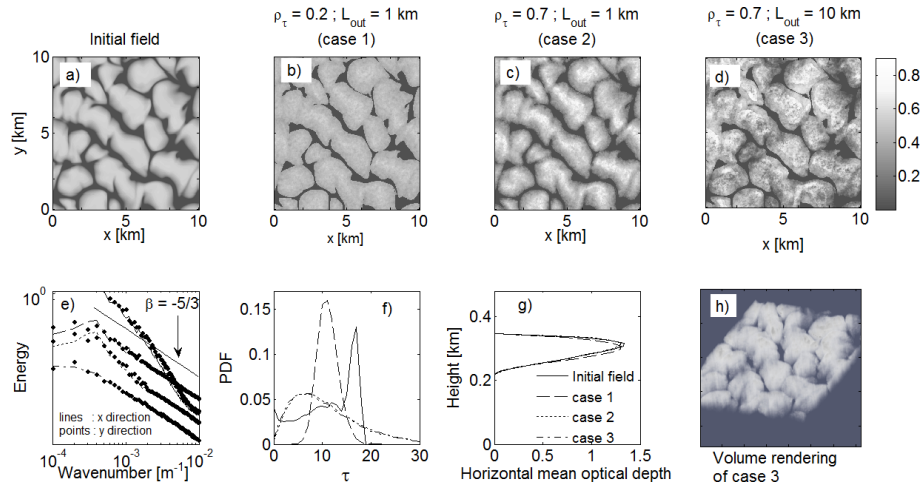
Fig. 10. (a) Pseudo albedo estimated from optical depth (initial field) simulated in the step 1 by 3DCLOUD for the DYCOMS2-RF01 case (see Fig. 7c), **(b)**, **(c)** and **(d)** pseudo albedo adjusted in the step 2 of 3DCLOUD for different values of the inhomogeneity parameter ρ_τ and of the outer scale L_{out}. **(e)** Mean power spectra of optical depth along x and y directions. The power spectra are scaled for better visualization. **(f)** Probability density function of optical depth, **(g)** mean vertical profiles of horizontally averaged optical depth and **(h)** volume rendering of optical depth for the case 3. ρ_τ and L_{out} are 0.2 and 1 km for case 1, 0.7 and 1 km for case 2 and 0.7 and 10 km for case 3, respectively. Solid lines, dotted lines, dashed lines and dash-dot lines indicate initial field, case 1, case 2 and case 3 fields, respectively.
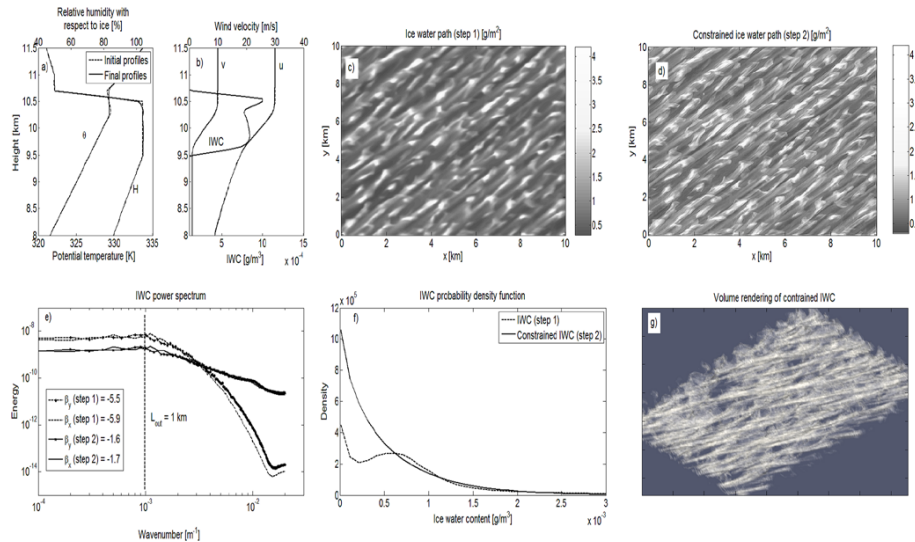
Fig. 11. Idealized vertical profiles assimilated (dashed lines) and simulated (solid lines) by 3DCLOUD during the step 1 of **(a)** the potential temperature and relative humidity and of **(b)** the horizontal velocity components and the ice water content (IWC), **(c)** ice water path (IWP) simulated by 3DCLOUD in step 1, **(d)** IWP simulated by 3DCLOUD in step 2, **(e)** mean power spectra of IWC along x and y directions after the step 1 and the step 2. **(f)** IWC probability density functions after the step 1 and the step 2. **(g)** IWC volume rendering after the step 2. ρ_{IWC} is set to 1 and L_{out} is set to 1 km.